THE ASTROPHYSICAL JOURNAL, 571:654–664, 2002 June 1
© 2002. The American Astronomical Society. All rights reserved. Printed in U.S.A.

A UNIFORM ANALYSIS OF THE Lyα FOREST AT $z = 0$–5. IV. THE CLUSTERING AND EVOLUTION OF CLOUDS AT $z \leq 1.7$

ADAM DOBRZYCKI
Harvard-Smithsonian Center for Astrophysics, 60 Garden Street, MS 70, Cambridge, MA 02138; adobrzycki@cfa.harvard.edu

AND

JILL BECHTOLD, JENNIFER SCOTT, AND MIWA MORITA
Steward Observatory, University of Arizona, Tucson, AZ 85721; jbechtold@as.arizona.edu, jscott@as.arizona.edu, mmorita@as.arizona.edu
Received 2001 July 25; accepted 2002 February 1

ABSTRACT

We present results on the evolution and clustering of Lyα lines at low redshift as part of our series "A Uniform Analysis of the Lyα Forest at $z = 0$–5." The sample analyzed in this paper contains 1298 Lyα absorption lines from 165 quasar spectra mined from the archives of the Faint Object Spectrograph on the *Hubble Space Telescope* (*HST*). Our sample extends to $z \approx 1.7$, slightly higher than the sample analyzed by the *HST* Quasar Absorption Line Key Project. We confirm the result from the Key Project that the number density evolution of Lyα lines at low redshifts can be described by a power law that is significantly flatter than that found at high z. We find that the evolution is somewhat steeper than obtained previously. Specifically, we find $\gamma = 0.54 \pm 0.21$ for lines with equivalent widths greater than 0.24 Å and $\gamma = 0.60 \pm 0.14$ using a variable equivalent width threshold. We find that the difference between our and Key Project results is likely attributable to different redshift coverage of the two samples. The results concerning the number density evolution are not significantly affected if one includes Lyα lines which are members of metal systems. Object-to-object fluctuations in the number of lines detected are small, indicating a high degree of uniformity in the intergalactic medium on large scales. We find marginal evidence that weak and strong lines undergo different evolution. We find weak clustering for Lyα lines at velocity separations $\Delta V \leq 500$ km s^{-1}, weaker than the level predicted from an earlier analysis by Ulmer of a small subsample of the Key Project data. We see no correlations for metal system–Lyα forest or extensive metal system–Lyα forest combinations.

Subject headings: intergalactic medium — quasars: absorption lines

On-line material: machine-readable table

1. INTRODUCTION

This paper is a continuation of the project of the analysis of Lyα absorption lines covering the range of redshifts, $z = 0$–5. The first two papers in this series (Scott, Bechtold, & Dobrzycki 2000, hereafter Paper I; Scott et al. 2000, hereafter Paper II) presented the analysis of intermediate-resolution ground-based data. This and accompanying papers (Bechtold et al. 2002, hereafter Paper III; Scott et al. 2002, hereafter Paper V) report the analysis of *Hubble Space Telescope* (*HST*) Faint Object Spectrograph (FOS; Ford & Hartig 1990) archival spectra.

Paper III describes the FOS data reductions, absorption line analysis, and line identification procedure. In this paper we present the distribution and clustering properties of the Lyα absorption lines.

All data analyzed in this and other papers from this series can be accessed from our Web pages.[1]

2. THE Lyα ABSORPTION LINE SAMPLE

From data presented in Paper III, we selected all spectra suitable for the analysis of the Lyα forest. We excluded spectra observed with A-1 aperture before installation of COSTAR, broad-absorption line quasars, and quasars observed in spectropolarimetry mode (see Paper III). In cases where two images of a gravitationally lensed quasar were observed, or a close pair of quasars or grouping of quasars were observed, we included only one line of sight, choosing the spectra with the highest signal-to-noise.

For detailed discussion on the detection significance and completeness in our sample, and on the identification of metal lines, see § 2 of Paper III.

In total, the sample analyzed in this paper contains spectra of 165 quasars (Table 1). The spectral resolution of all the data is 230–280 km s^{-1} FWHM. Of those 165 quasars, 63 were analyzed by Weymann et al. (1998) as part of the *HST* Quasar Absorption Line Key Project (Bahcall et al. 1993, 1996; Schneider et al. 1993; Jannuzi et al. 1998; Weymann et al. 1998). The sixty-fourth object in Weymann et al. sample, PG 2302+029, is a broad absorption line quasar (Jannuzi et al. 1996) and was excluded from our sample (as well as from samples 6–10 in Weymann et al.).

We selected the sample of the absorption lines for further analysis using the following criteria:

1. The detection significance for the line has to be greater than 5 σ.
2. A line cannot be identified as a heavy element absorption feature. Regions within 300 km s^{-1} of the centers of metal absorption lines were excluded from the analysis.
3. Whenever a Lyα "forest" sample was called for, we excluded Lyα lines identified as members of heavy element systems and regions within 300 km s^{-1} from such lines.
4. We excluded lines lying blueward from the location of the Lyβ emission line, to avoid confusion with the Lyβ lines from higher redshift Lyα systems.

[1] See http://hea-www.harvard.edu/QEDT/QuasarSpectra/ or http://lithops.as.arizona.edu/~jill/QuasarSpectra/.

TABLE 1

HST/FOS Quasar Sample

Designation	z	α_{1950}	δ_{1950}	Object Name	z_{beg}[a]	z_{end}[b]	U/V/W[c]
Q0002+0507	1.900	00 02 46.4	+05 07 29	UM 18	1.447	1.693	W
Q0003+1553	0.450	00 03 25.1	+15 53 07	0003+15	0.223	0.450	W
Q0003+1955	0.025	00 03 45.3	+19 55 28	Mrk 335	0.006	0.025	
Q0007+1041	0.089	00 07 56.7	+10 41 47	III Zw 2	0.007	0.089	
Q0015+1612	0.553	00 15 56.7	+16 12 46	QSO 0015+162	0.310	0.553	
Q0017+0209	0.401	00 17 51.1	+02 09 46	Q0017+0209	0.330	0.401	
Q0024+2225	1.108	00 24 38.6	+22 25 23	NAB 0024+22	0.779	1.108	W
Q0026+1259	0.142	00 26 38.1	+12 59 29	PG 0026+12	0.001	0.142	
Q0042+1010	0.583	00 42 22.8	+10 10 28	MC 0042+101	0.368	0.583	
Q0043+0354	0.384	00 43 12.6	+03 54 00	PG 0043+039	0.354	0.384	W
Q0044+0303	0.624	00 44 31.5	+03 03 32	PKS 0044+030	0.370	0.624	W
Q0050+1225	0.061	00 50 58.0	+12 25 20	I Zw 1	0.007	0.061	
Q0100+0205	0.394	01 00 38.6	+02 05 04	0100+0205	0.295	0.394	
Q0102−2713	0.780	01 02 16.6	−27 13 12	CT 336	0.502	0.780	V
Q0107−0235	0.948	01 07 40.3	−02 35 51	Q0107−025A	0.644	0.899	
Q0107−1537	0.861	01 07 03.2	−15 37 50	QSO 0107−156	0.831	0.861	
Q0117+2118	1.493	01 17 34.7	+21 18 02	PG 0117+213	1.103	1.493	W
Q0121−5903	0.047	01 21 51.2	−59 03 59	FAIRALL 9	0.013	0.047	
Q0122−0021	1.070	01 22 55.3	−00 21 31	PKS 0122−003	0.747	1.070	UW
Q0137+0116	0.260	01 37 22.9	+01 16 35	PHL 1093	0.234	0.260	
Q0159−1147	0.669	01 59 30.4	−11 47 00	3C 57	0.408	0.669	W
Q0214+1050	0.408	02 14 26.8	+10 50 18	PKS 0214+10	0.295	0.408	
Q0219+4248	0.444	02 19 30.1	+42 48 30	3C 66A	0.218	0.444	
Q0232−0415	1.450	02 32 36.6	−04 15 10	PKS 0232−04	1.067	1.450	W
Q0254−3327B.....	1.915	02 54 39.4	−33 27 24	PKS 0254−334	1.460	1.693	
Q0302−2223	1.400	03 02 35.7	−22 23 29	1E 0302−223	1.025	1.397	
Q0333+3208	1.258	03 33 22.5	+32 08 36	NRAO 140	0.905	1.251	
Q0349−1438	0.616	03 49 09.6	−14 38 06	3C 95	0.364	0.616	UW
Q0355−4820	1.005	03 55 52.5	−48 20 48	0355−4820	0.828	1.005	
Q0405−1219	0.574	04 05 27.5	−12 19 31	PKS 0405−12	0.328	0.574	W
Q0414−0601	0.781	04 14 49.3	−06 01 05	PKS 0414−06	0.503	0.781	W
Q0420−0127	0.915	04 20 43.5	−01 27 29	PKS 0420−01	0.830	0.915	
Q0421+0157	2.044	04 21 32.7	+01 57 32	PKS 0421+01	1.568	1.685	
Q0424−1309	2.159	04 24 47.7	−13 09 33	PKS 0424−13	1.678	1.693	
Q0439−4319	0.593	04 39 42.8	−43 19 24	PKS 0439−433	0.344	0.593	W
Q0454−2203	0.534	04 54 01.2	−22 03 49	PKS 0454−22	0.294	0.534	
Q0454+0356	1.345	04 54 09.0	+03 56 14	PKS 0454+039	0.979	1.345	
Q0518−4549	0.035	05 18 23.6	−45 49 43	PKS 0518−45	0.002	0.035	
Q0624+6907	0.374	06 24 35.3	+69 07 03	HS 0624+6907	0.159	0.374	W
Q0637−7513	0.656	06 37 23.5	−75 13 37	PKS 0637−75	0.397	0.656	W
Q0742+3150	0.462	07 42 30.8	+31 50 15	B20742+318	0.329	0.462	W
Q0743−6719	1.511	07 43 22.3	−67 19 07	PKS 0743−67	1.119	1.511	W
Q0823−2220	0.910	08 23 50.0	−22 20 34	PKS 0823−22	0.828	0.910	
Q0827+2421	0.935	08 27 54.4	+24 21 07	B20827+24	0.831	0.935	
Q0844+3456	0.064	08 44 34.0	+34 56 07	TON 951	0.007	0.064	
Q0848+1623	1.936	08 48 53.7	+16 23 40	Q0848+163	1.479	1.694	
Q0850+4400	0.513	08 50 13.5	+44 00 24	US 1867	0.327	0.513	W
Q0916+5118	0.553	09 16 30.1	+51 18 52	NGC 2841 UB3	0.310	0.553	W
Q0935+4141	1.937	09 35 48.8	+41 41 55	PG 0935+416	1.478	1.693	
Q0945+4053	1.252	09 45 50.1	+40 53 43	4C 40−24	0.900	1.252	
Q0947+3940	0.206	09 47 44.9	+39 40 54	PG 0947+396	0.018	0.206	
Q0953+4129	0.239	09 53 48.3	+41 29 40	PG 0953+414	0.045	0.239	W
Q0955+3238	0.533	09 55 25.5	+32 38 23	3C 232	0.293	0.533	W
Q0957+5608A	1.414	09 57 57.4	+56 08 22	0957+561A	1.041	1.414	
Q0958+5509	1.750	09 58 08.2	+55 09 06	Mrk 132	1.327	1.694	
Q0959+6827	0.773	09 59 09.7	+68 27 47	0959+68W1	0.496	0.773	W
Q1001+0527	0.161	10 01 43.3	+05 27 34	PG 1001+054	0.002	0.161	
Q1001+2239	0.974	10 01 58.5	+22 39 54	PKS 1001+22	0.830	0.974	
Q1001+2910	0.329	10 01 10.7	+29 10 08	TON 28	0.121	0.329	W
Q1007+4147	0.611	10 07 26.1	+41 47 25	4C 41.21	0.359	0.611	W
Q1008+1319	1.287	10 08 29.9	+13 19 00	PG 1008+133	0.930	1.287	W
Q1010+3606	0.070	10 10 07.4	+36 06 15	CSO 251	0.004	0.070	
Q1017+2759	1.928	10 17 07.8	+27 59 06	TON 34	1.470	1.693	
Q1026−0045A	1.437	10 26 01.7	−00 45 22	Q1026−0045−A	1.056	1.437	
Q1026−0045B.....	1.530	10 26 03.6	−00 45 06	Q1026−0045−B	1.141	1.530	

TABLE 1—*Continued*

Designation	z	α_{1950}	δ_{1950}	Object Name	z_{beg}[a]	z_{end}[b]	U/V/W[c]
Q1038+0625.....	1.270	10 38 41.0	+06 25 58	4C 06.41	0.915	1.270	W
Q1049−0035.....	0.357	10 49 18.1	−00 35 21	PG 1049−005	0.327	0.357	W
Q1055+2007.....	1.110	10 55 37.6	+20 07 55	PKS 1055+20	0.830	1.110	
Q1100+7715.....	0.311	11 00 27.5	+77 15 08	3C 249−1	0.106	0.311	W
Q1104+1644.....	0.634	11 04 36.7	+16 44 16	MC 1104+167	0.379	0.634	W
Q1114+4429.....	0.144	11 14 20.0	+44 29 57	PG 1114+445	0.002	0.144	
Q1115+0802A1 ..	1.722	11 15 41.5	+08 02 23	PG 1115+080A1	1.309	1.694	
Q1115+4042.....	0.154	11 15 45.9	+40 42 19	PG 1115+407	0.002	0.154	
Q1116+2135.....	0.177	11 16 30.2	+21 35 43	PG 1116+215	0.004	0.177	W
Q1118+1252.....	0.685	11 18 53.5	+12 52 43	MC 1118+12	0.422	0.685	
Q1130+1108.....	0.510	11 30 55.0	+11 08 57	1130+106Y	0.337	0.510	W
Q1136−1334.....	0.557	11 36 38.6	−13 34 05	PKS 1136−135	0.334	0.557	W
Q1137+6604.....	0.652	11 37 09.4	+66 04 27	3C 263.0	0.394	0.652	UW
Q1138+0204.....	0.383	11 38 47.8	+02 04 41	Q1138+0204	0.351	0.383	
Q1146+1104B.....	1.010	11 46 09.8	+11 04 37	1146+111B	0.696	0.899	
Q1146+1106C.....	1.010	11 46 04.9	+11 06 57	1146+111C	0.696	0.891	
Q1148+5454.....	0.969	11 48 42.6	+54 54 13	1148+5454	0.661	0.969	
Q1150+4947.....	0.334	11 50 48.1	+49 47 50	LB 2136	0.295	0.334	
Q1156+2123.....	0.349	11 56 52.3	+21 23 38	TEX 1156+213	0.296	0.349	
Q1156+2931.....	0.729	11 56 57.9	+29 31 25	4C 29.45	0.459	0.729	
Q1206+4557.....	1.158	12 06 26.6	+45 57 17	PG 1206+459	0.821	1.158	
Q1211+1419.....	0.085	12 11 45.0	+14 19 52	PG 1211+1431	0.012	0.085	
Q1214+1804.....	0.375	12 14 16.8	+18 04 44	Q1214+1804	0.344	0.373	
Q1215+6423.....	1.288	12 15 17.1	+64 23 46	4C 64−15	0.931	1.288	
Q1216+0655.....	0.334	12 16 47.8	+06 55 17	PG 1216+069	0.126	0.334	W
Q1216+5032A	1.450	12 16 13.5	+50 32 15	HS 1216+5032A	1.067	1.450	
Q1219+0447.....	0.094	12 19 04.7	+04 47 03	1219+047	0.006	0.094	
Q1226+0219.....	0.158	12 26 33.2	+02 19 42	3C 273	0.002	0.158	UW
Q1229−0207.....	1.045	12 29 26.0	−02 07 32	PKS 1229−02	0.725	1.045	
Q1241+1737.....	1.273	12 41 41.0	+17 37 28	PG 1241+176	0.918	1.273	W
Q1247+2647.....	2.043	12 47 39.1	+26 47 26	PG 1247+267	1.568	1.694	
Q1248+3032.....	1.061	12 48 00.2	+30 32 58	B21248+30	0.831	1.061	V
Q1248+3142.....	1.020	12 48 25.4	+31 42 11	CSO 173	0.704	0.899	V
Q1248+4007.....	1.030	12 48 26.6	+40 07 58	PG 1248+401	0.713	1.030	W
Q1249+2929.....	0.820	12 49 59.6	+29 29 38	CSO 176	0.536	0.820	V
Q1250+3122.....	0.780	12 50 52.9	+31 22 06	CSO 179	0.502	0.780	V
Q1252+1157.....	0.871	12 52 07.7	+11 57 21	PKS 1252+11	0.579	0.871	W
Q1257+3439.....	1.375	12 57 26.6	+34 39 31	B2011257+34	1.004	1.375	VW
Q1258+2835.....	1.355	12 58 36.6	+28 35 52	QSO 1258+285	0.987	1.355	
Q1259+5918.....	0.472	12 59 08.3	+59 18 14	PG 1259+593	0.242	0.472	UW
Q1302−1017.....	0.286	13 02 55.9	−10 17 17	PKS 1302−102	0.085	0.286	W
Q1305+0658.....	0.602	13 05 22.6	+06 58 14	3C 281	0.352	0.602	
Q1309+3531.....	0.184	13 09 58.4	+35 31 15	PG 1309+355	0.007	0.184	V
Q1317+2743.....	1.022	13 17 34.4	+27 43 51	TON 153	0.706	1.022	UVW
Q1318+2903.....	0.549	13 18 54.7	+29 03 01	TON 156	0.319	0.549	V
Q1320+2925.....	0.960	13 20 59.9	+29 25 45	TON 157	0.654	0.958	V
Q1322+6557.....	0.168	13 22 08.5	+65 57 24	PG 1322+659	0.002	0.168	
Q1323+6530.....	1.618	13 23 48.6	+65 30 47	4C 65.15	1.209	1.618	
Q1327−2040.....	1.169	13 27 24.3	−20 40 48	PKS 1327−206	0.831	1.169	
Q1328+3045.....	0.849	13 28 49.7	+30 45 58	3C 286.0	0.560	0.849	V
Q1329+4117.....	1.930	13 29 29.8	+41 17 23	PG 1329+412	1.472	1.694	
Q1333+1740.....	0.554	13 33 36.8	+17 40 30	PG 1333+176	0.347	0.554	W
Q1338+4138.....	1.219	13 38 52.1	+41 38 22	PG 1338+416	0.872	1.213	W
Q1351+3153.....	1.326	13 51 51.3	+31 53 45	B21351+31	0.963	1.326	
Q1351+6400.....	0.088	13 51 46.4	+64 00 29	PG 1351+64	0.008	0.088	
Q1352+0106.....	1.117	13 52 25.6	+01 06 51	PG 1352+011	0.790	1.117	UW
Q1352+1819.....	0.152	13 52 12.6	+18 19 58	PG 1352+183	0.002	0.152	
Q1354+1933.....	0.719	13 54 42.2	+19 33 43	PKS 1354+19	0.450	0.719	W
Q1404+2238.....	0.098	14 04 02.5	+22 38 03	PG 1404+226	0.002	0.098	
Q1407+2632.....	0.944	14 07 07.8	+26 32 30	PG 1407+265	0.640	0.944	W
Q1415+4509.....	0.114	14 15 04.7	+45 09 56	PG 1415+451	0.002	0.114	
Q1416+0642.....	1.436	14 16 38.8	+06 42 20	3C 298	1.055	1.436	
Q1424−1150.....	0.806	14 24 56.0	−11 50 25	PKS 1424−118	0.524	0.806	W
Q1425+2645.....	0.366	14 25 21.9	+26 45 39	B21425+26	0.295	0.366	
Q1427+4800.....	0.221	14 27 54.0	+48 00 44	PG 1427+480	0.030	0.221	
Q1435−0134.....	1.310	14 35 13.3	−01 34 13	Q1435−0134	0.949	1.304	

TABLE 1—*Continued*

Designation	z	α_{1950}	δ_{1950}	Object Name	z_{beg}[a]	z_{end}[b]	U/V/W[c]
Q1435+6349	2.068	14 35 37.3	+63 49 36	S41435+638	1.589	1.693	
Q1440+3539	0.077	14 40 04.6	+35 39 07	1440+3539	0.004	0.077	
Q1444+4047	0.267	14 44 50.2	+40 47 38	PG 1444+407	0.069	0.267	
Q1512+3701	0.371	15 12 47.4	+37 01 55	B21512+37	0.330	0.371	W
Q1517+2356	1.903	15 17 08.3	+23 56 53	LB 9612	1.449	1.694	
Q1517+2357	1.834	15 17 02.2	+23 57 44	LB 9605	1.391	1.694	
Q1521+1009	1.324	15 21 59.9	+10 09 02	PG 1522+101	0.962	1.324	
Q1538+4745	0.770	15 38 01.0	+47 45 10	PG 1538+477	0.493	0.770	W
Q1544+4855	0.400	15 44 00.2	+48 55 25	1543+4855	0.182	0.400	
Q1618+1743	0.555	16 18 07.4	+17 43 30	3C 334.0	0.315	0.555	W
Q1622+2352	0.927	16 22 32.3	+23 52 01	3C 336.0	0.627	0.927	
Q1626+5529	0.133	16 26 51.5	+55 29 04	PG 1626+554	0.002	0.133	
Q1630+3744	1.400	16 30 15.2	+37 44 08	1630+377	1.094	1.478	
Q1634+7037	1.337	16 34 51.8	+70 37 37	PG 1634+706	0.978	1.337	UW
Q1641+3954	0.595	16 41 17.7	+39 54 10	3C 345	0.346	0.595	
Q1704+6048	0.371	17 04 03.5	+60 48 30	3C 351.0	0.160	0.371	UW
Q1715+5331	1.940	17 15 30.3	+53 31 27	PG 1715+535	1.481	1.694	
Q1718+4807	1.084	17 18 17.9	+48 07 10	PG 1718+481	0.758	1.084	
Q1803+7827	0.680	18 03 39.4	+78 27 54	S51803+78	0.417	0.680	
Q1821+6419	0.297	18 21 44.1	+64 19 32	H1821+643	0.094	0.297	UW
Q1845+7943	0.056	18 45 37.5	+79 43 06	3C 390.3	0.002	0.056	
Q2112+0556	0.457	21 12 47.6	+05 56 10	PG 2112+059	0.309	0.457	
Q2128−1220	0.501	21 28 52.9	−12 20 21	PKS 2128−12	0.310	0.501	W
Q2135−1446	0.200	21 35 01.2	−14 46 27	PKS 2135−147	0.013	0.200	
Q2141+1730	0.213	21 41 13.9	+17 30 02	OX 1692141+175	0.023	0.213	
Q2145+0643	0.990	21 45 36.2	+06 43 41	PKS 2145+067	0.679	0.990	UW
Q2243−1222	0.630	22 43 39.9	−12 22 40	PKS 2243−123	0.376	0.630	W
Q2251−1750	0.068	22 51 25.9	−17 50 54	MR 2251−178	0.002	0.068	
Q2251+1120	0.323	22 51 40.7	+11 20 40	PKS 2251+113	0.116	0.323	W
Q2251+1552	0.859	22 51 29.7	+15 52 54	3C 454.3	0.569	0.859	UW
Q2300−6823	0.512	23 00 27.9	−68 23 47	PKS 2300−683	0.309	0.512	W
Q2340−0339	0.896	23 40 22.6	−03 39 05	PKS 2340−036	0.600	0.896	W
Q2344+0914	0.672	23 44 03.9	+09 14 06	PKS 2344+092	0.411	0.672	W
Q2352−3414	0.706	23 52 50.8	−34 14 37	PKS 2352−342	0.439	0.706	W

NOTE.—Units of right ascension are hours, minutes, and seconds, and units of declination are degrees, arcminutes, and arcseconds. Table 1 is also available in machine-readable form in the electronic edition of the *Astrophysical Journal*.

[a] Lower end of the analyzed redshift range.

[b] Upper end of the analyzed redshift range.

[c] (U) object in Ulmer 1996 sample. (V) Object in Vanden Berk et al. 1999 sample. (W) Object in Weymann et al. 1998 sample.

Please note that these criteria are more conservative than those of the *HST* Key Project. The sample contains 1298 lines if all Lyα lines (forest and metal systems) are selected, and 1157 Lyα forest lines. Figure 1 shows the rest equivalent width, W_{λ_0}, defined as $W_{\lambda_0} = W_{\lambda(\mathrm{obs})}/(1+z)$, of all Ly$\alpha$ lines versus redshift, z. Equivalent widths were measured from Gaussian fits to significant absorption features (see Paper III). This plot has not been corrected for the relative sensitivity for detection at each redshift and is only intended to show the redshift distribution of the sample.

Figure 2 shows the histogram of rest equivalent widths of lines in the full Lyα sample. The shaded area shows the Lyα lines with detected metal absorption. Figure 2 clearly shows that lines associated with metal systems begin to compose a significant part of the sample for rest equivalent widths greater than $\sim$1 Å. We cannot rule out the possibility that some of the lines in our sample are in fact unidentified metal system lines. However, we found that the exclusion from the analysis of all lines with $W_{\lambda_0} > 1$ Å—which, in view of Figure 2, are the prime suspects for being unrecognized metal lines—produced negligible differences in the number density evolution results.

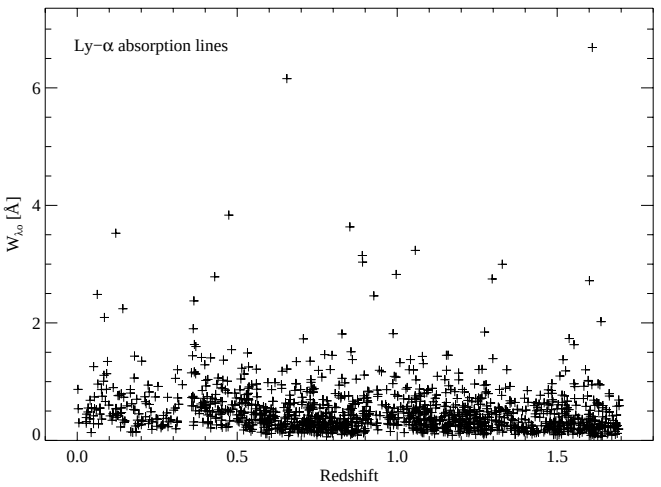


FIG. 1.—Equivalent widths of all Lyα lines, forest and metal systems, vs. redshift.

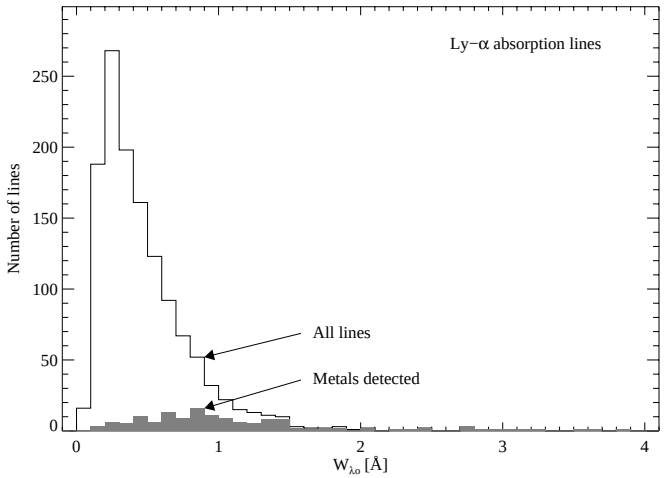


FIG. 2.—Histogram of rest equivalent widths for Lyα lines. The shaded area shows the fraction of Lyα lines from heavy element systems.

Figure 3 shows the comparison of redshift coverage in our sample with the Weymann et al. (1998) sample. The upper panel shows the combined path length available for study in both samples as a function of redshift, while the lower panel shows the number of available lines. The notable differences are that (1) our sample extends to $z \sim 1.8$, while the Key Project sample effectively ends at $z \sim 1.5$; (2) our sample contains considerably more lines in the $z = 1.0$–1.5 range; and (3) our sample by definition excludes lines below Lyβ emission line, while the Key Project sample does not.

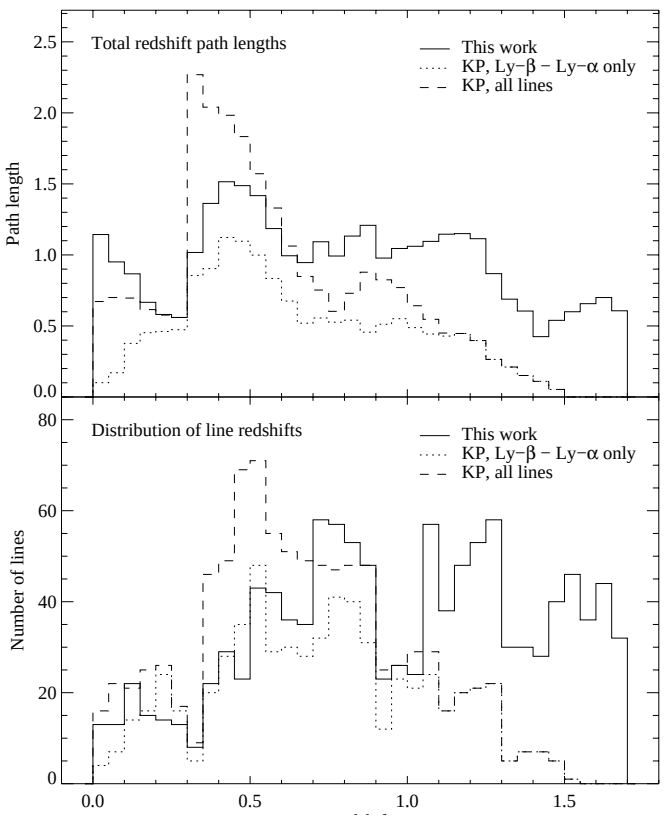


FIG. 3.—Histogram of total redshift path length (*upper panel*) and lines (*lower panel*) vs. redshift in our full Lyα forest sample (*solid line*), Weymann et al. (1998) full sample (*dashed line*), and Weymann et al. Lyβ–Lyα only sample (*dotted line*).

We note that we did not attempt to remove the flat-field features in the FOS spectra, which the Key Project went to great lengths to do (Schneider et al. 1993; Jannuzi et al. 1998). We identify 38 of their 141 confirmed flat-field features as lines with significance greater than 5 σ (Paper III). However, only nine of those features lie in the Lyα forest. Simple extrapolation of those numbers to the sample analyzed here would indicate that roughly 24 lines out of our total sample of 1298, or less than 2%, are spurious. However, even this low number is likely overestimated, since majority of redshift path in our sample that is added to the Key Project sample (see Fig. 3) is in regions covered by G130H and G270H gratings, which have less (none in the case of G130H, actually) identified flat-field features than grating G190H (Jannuzi et al. 1998). Those should have a negligible effect on our results.

3. PROPERTIES OF Lyα ABSORBERS AT $z \lesssim 1.7$

We parameterized the distribution of individual clouds using

$$\frac{\partial^2 \mathcal{N}}{\partial z \partial W_{\lambda_0}} = \mathcal{A}_0 W_\star^{-1} (1+z)^\gamma \exp\left(-\frac{W_{\lambda_0}}{W_\star}\right) \qquad (1)$$

where $\mathcal{A}_0$, γ, and $W_\star$ are the distribution parameters. For a nonevolving population of clouds $1/2 \leq \gamma \leq 1$, depending on the value of q_0 (Peterson 1978). It is well established that γ is significantly greater than 1 at $z \gtrsim 1.7$, indicating strong evolution (e.g., Bajtlik, Duncan, & Ostriker 1988; Lu, Wolfe, & Turnshek 1991; Bechtold 1994; Kim et al. 1997; Paper I). However, the *HST* Quasar Absorption Line Key Project and other studies showed that γ is less then 1 at $z \lesssim 1.7$, consistent with the no-evolution case (Bahcall et al. 1993, 1996; Weymann et al. 1998; Vanden Berk et al. 1999; Impey, Petry, & Flint 1999).

The proximity effect (Bajtlik et al. 1988; Bechtold 1994; Paper II) at high redshift causes the derived value of γ to depend strongly on the inclusion or exclusion of lines with $z_{\rm abs} \sim z_{\rm em}$. However, the proximity effect is not expected to influence the results as significantly at low redshift for a few reasons. First, the overall number density of absorbers per unit redshift is smaller than at high redshift, and so the expected number of lines affected will also be small. Second, the quasars used at low redshift are intrinsically fainter on average than the quasars observed at high z, and thus it is expected that their influence at their environment will also be less prominent (see Paper V). We determined the distribution parameters both including and excluding lines with "ejection velocity" $V_{\rm ej}$, velocity displacement from the emission redshift of the quasar, greater than 3000 km s^{-1}. A detailed analysis of the proximity effect is presented in Paper V.

3.1. *The Method*

We estimated the parameters $\mathcal{A}_0$, γ, and $W_\star$ from equation (1) for the whole FOS sample and several subsamples. We developed and utilized a computer code, based on the algorithm from Murdoch et al. (1986; their eqs. [A2a] and [A8a] corrected), modified so that the integral in equation (A2) of Murdoch et al., which cannot be calculated analytically in the case of variable threshold, is derived

numerically. The Murdoch et al. method consists of solving for γ and $W_\star$ by finding the roots of the derivatives of the log of the likelihood function describing equation (1) with respect to γ and $W_\star$. Uncertainties in each parameter are found from a parabolic fit to $\ln L$ such that 1 σ corresponds to $\ln L = \ln L_{\max} - 1/2$. The normalization, $\mathscr{A}_0$, is calculated by dividing the total number of lines by the sum of the integral of equation (1) over the redshift paths in all quasars:

$$\mathscr{A}_0 = \mathscr{N} \times \left[\sum_q \int_{z_{\min}^q}^{z_{\max}^q} (1+z)^\gamma dz \right]^{-1} . \quad (2)$$

for the considered sample. For each run of our program, we tested the goodness of fit of the outcome using the Kolmogorov-Smirnoff test.

This treatment of the normalization differs slightly from that of the *HST* Key Project. We and the Key Project both solve for γ and $W_\star$ using all lines above some rest equivalent width that is either fixed to some constant value or varied according to the signal-to-noise ratio in each spectral region. Weymann et al. (1998) determine the normalization, denoted dN/dz in their Table 2, explicitly in the maximum-likelihood solution rather than by using equation (2). Each dN/dz-value listed in their table is the local line density relative to the local density of lines above 0.24 Å, regardless of the limiting equivalent width of the sample used. In our software, this relative scaling is not done. In other words, we always normalize to the stated constant rest equivalent width limit and do not quote a value of $\mathscr{A}_0$ for the case of a variable rest equivalent width limit.

3.2. *Results*

3.2.1. *Number Density Evolution*

Table 2 presents a summary of our estimates of the parameters from equation (1) in several subsamples of the data set. The main result, seen clearly in Table 2, is that in all cases the value of the evolution index, γ, is within few tenths of 0.5, significantly lower than the value estimated from ground-based samples of Lyα forest lines at redshifts greater than $\sim$1.7. Our values are consistent with the "no-evolution" expectations. We show the results for the $W_{\lambda_0} \geq 0.24$ Å, $V_{\rm ej} \geq 3000$ km s^{-1} sample in Figure 4. The values of the K-S probability show that the power law is an excellent approximation of the distribution of lines at the redshift range covered in our sample. Note that this disagrees with the result of Kim, Cristiani, & D'Odorico (2001), who found that the break in $d\mathscr{N}/dz$ slope occurred around $z \sim 1.2$.

The results appear to depend only weakly on whether the Lyα lines from metal systems are included in the sample. Also, it can be seen in Table 2 that taking the proximity effect into account—by excluding the lines with $V_{\rm ej} < 3000$ km s^{-1}—results in an insignificant change in the estimates of the number density evolution index; the difference is of the order of 1 σ or less.

3.2.2. *Comparison with HST QSOAL Key Project*

The results agree qualitatively with the findings of the *HST* QSOAL Key Project. Weymann et al. (1998) have analyzed the complete Key Project Lyα absorption line sample and also found that the evolution index, γ, is smaller than the one found for high-redshift samples. However, their values of γ for various Lyα subsamples range from -0.03 to $+0.26$ with uncertainties of $\sim$0.20. The values of γ that we find from our total FOS sample are larger than those found by the Key Project by $\sim$1.9 σ in the case of the constant, 0.24 Å equivalent width threshold and by $\sim$4.5 σ in the case of a variable equivalent width threshold.

A comparison of these two results is shown in Figure 4, where we show our data and fit for $W_{\lambda_0} \geq 0.24$ Å (*solid line*), and the $d\mathscr{N}/dz$ versus z curve (*dotted line*) for a comparable sample from Weymann et al. (1998; their sample 5, which had $\mathscr{A}_0 = 30.7$ and $\gamma = 0.15 \pm 0.23$). We see a comparable number of lines per unit redshift at low z, but slightly (around 15%) more lines at $z \approx 1.5$.

There are a few effects that may account for the discrepancy. As noted earlier (see Fig. 3), our sample has larger redshift coverage and contains markedly more lines at $z = 1.0$–1.5. Also, our sample excludes lines below Lyβ emission line.

We determined the parameters of equation (1) in a subsample of our data, containing only the objects we had in common with the Key Project. The results were in very good

TABLE 2

MAXIMUM-LIKELIHOOD FITS FOR THE *HST*/FOS SAMPLE

A/F[a]	$W_{\rm thr}$[b] (Å)	$W_{\max}$[c] (Å)	$V_{\rm ej}$[d] (km s^{-1})	Δz[e]	$\mathscr{N}$	γ	$W_\star$ (Å)	$\mathscr{A}_0$[f]	$P_{\rm KS}$[g]
A.....	VAR	∞	0	32.96	1298	0.65±0.12	0.300±0.008	...	0.85
A.....	VAR	∞	3000	29.48	1147	0.73±0.13	0.293±0.008	...	0.74
F.....	VAR	∞	0	32.45	1157	0.62±0.13	0.229±0.006	...	0.88
F.....	VAR	∞	3000	29.07	1038	0.60±0.14	0.229±0.006	...	0.88
A.....	0.24	∞	3000	14.24	622	0.42±0.20	0.309±0.012	32.7	0.96
F.....	0.24	∞	3000	13.93	544	0.54±0.21	0.220±0.009	26.9	0.99
F.....	0.24	0.36	3000	13.93	223	0.38±0.32	...	12.3	0.56
F.....	0.36	∞	3000	19.98	437	0.62±0.21	0.218±0.010	25.8	0.93

[a] (A) All Lyα lines (forest and metal systems); (F) Lyα forest only.
[b] Rest equivalent width threshold.
[c] Upper limit for rest equivalent width.
[d] Minimum ejection velocity.
[e] Combined redshift path length in the sample.
[f] Scaled to refer to lines with $W_{\lambda_0} \geq 0.24$ Å.
[g] Kolmogorov-Smirnoff probability for the fit.

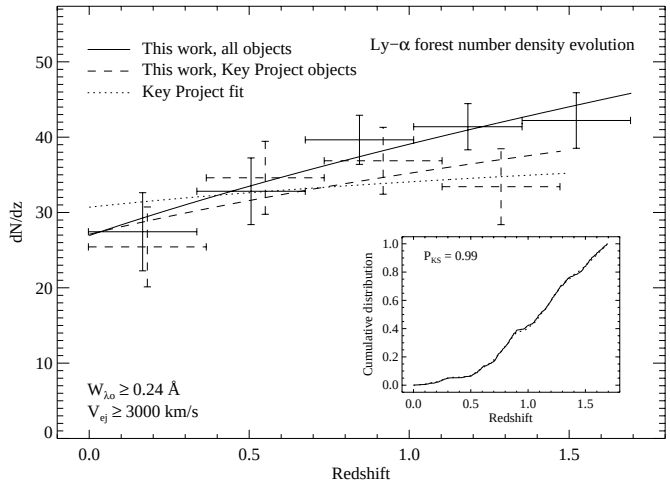


FIG. 4.—Number density evolution of Lyα lines for the $W_{\lambda_0} \geq 0.24$ Å, $V_{\rm ej} \geq 3000$ km s^{-1} sample. *Solid data points and line*: our results for the whole sample. *Dashed data points and curve*: our results for the sample limited to the Weymann et al. (1998) objects. *Dotted line*: fit from Weymann et al. (1998), their sample 5. The data are binned for presentation only; the lines show the fits to unbinned data. The inner box shows the comparison of cumulative distribution of lines in the sample (*solid line*) and eq. (1) integrated over the sample (*dashed line*).

agreement with Weymann et al. (1998); we show the data points and the fit on Figure 4. Specifically, we obtained $\gamma = 0.38 \pm 0.36$ for the $W_{\lambda_0} \geq 0.24$ Å sample, and $\gamma = 0.26 \pm 0.22$ for the variable threshold case, markedly lowering any discrepancy. Also, the results show the same qualitative behavior of lowering the value of γ when limiting the analysis to the Key Project objects.

The other effect that can influence the results is the exclusion of lines below Lyβ emission lines. In order to verify whether this can account for at least part of the discrepancy, we analyzed the Lyα line lists of the *HST* Key Project using our equivalent width threshold information and our metal system identifications for excluding spectral regions. Including identified Lyα lines blueward of Lyβ emission—as the Key Project did—we find $\gamma = -0.03 \pm 0.20$ and $\gamma = -0.10 \pm 0.29$, for variable and 0.24 Å thresholds, respectively, in good agreement with the Key Project results. Excluding lines blueward of Lyβ emission, we find $\gamma = -0.03 \pm 0.24$ and $\gamma = -0.01 \pm 0.32$ for variable and 0.24 Å thresholds, respectively, i.e., no significant difference in both cases. We thus conclude that exclusion or inclusion of lines below Lyβ does not affect the results and that the primary source of the discrepancy between our results and those of and Weyman et al. (1998) lies in the difference in the sample coverage.

It is known that $d\mathcal{N}/dz$ steepens around $z \sim 1.6$–1.8. It is obvious from Figure 5 of Weymann et al. (1998) that if they included the $z_{\rm em} = 1.9$ quasar UM 18 in their sample (it was excluded because of incomplete line identifications; note that this object is included in the sample presented here), then their derived distribution would have been considerably steeper, in agreement with our result. It is possible that this, combined with the fact that we have better coverage at the high-z end of the sample, contributes to our deriving larger γ than the Key Project. We note, however, that the fact that K-S test shows that for our sample the power law is an excellent approximation of the number density evolution over the entire redshift range of our sample, in apparent contradiction to what inclusion of UM 18 would do to the Key Project sample, in which case their fit to a single power law would likely become worse.

3.2.3. *Dependence of Evolution on Line Equivalent Width*

If the intergalactic medium evolves, then we expect that the observed γ could depend on equivalent width, or equivalently, the distribution of equivalent widths could be a function of redshift. Weymann et al. (1998) found a trend of increasing γ with increasing line strength in the Key Project data. However, Penton, Shull, & Stocke (2000) saw no difference in the evolution of strong and weak lines in the *HST*/GHRS sample.

Although the statistical significance is low, our results suggest that there appears to be a difference in the rate of evolution for weak and strong lines. In Figure 5 the solid line shows the evolution of the number density of absorbers for lines from one of the samples, with $W_{\lambda_0} \geq 0.24$ Å. On the same plot, we show the data and fits for two of its subsamples: the dashed line shows the sample with $W_{\lambda_0} \geq 0.36$ Å, the dotted line—$0.24 \leq W_{\lambda_0} < 0.36$ Å. As in other plots, the data have been arbitrarily binned solely for presentation; the lines show the fits to unbinned data.

While number densities of strong and weak lines seem to be comparable in the present epoch, there are more (by roughly 25%) strong lines at $z \approx 1.7$. In principle, the dividing line between those two subsamples lies near the point where Lyα lines leave the linear part of the curve of growth. Therefore, one could try to interpret this result as an indication that the two subsamples are in fact two different populations of absorbers. However, there are two reasons why we regard this result with caution and avoid drawing far-reaching conclusions. First, the result is marginal. Second, the same behavior would be expected to occur from line blending. Two blending effects associated with increased density of lines at larger z may affect the relative number of strong and weak lines: (1) two lines, both above the threshold, may blend into features indistinguishable from strong lines ("blending-out"), or (2) two weak lines, both with W_{λ_0} below the threshold, may blend, resulting in a feature

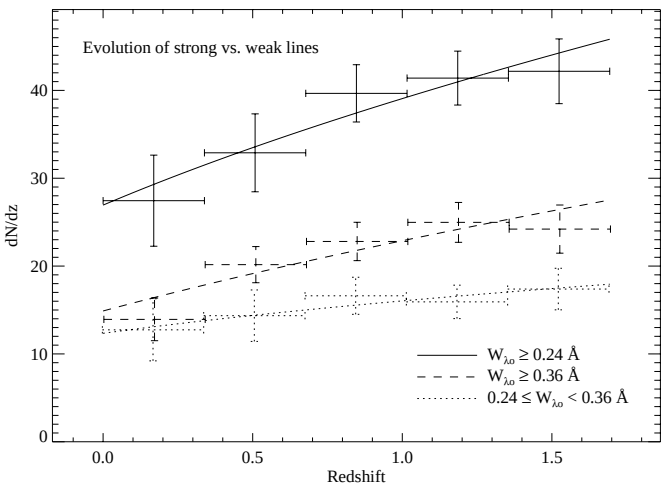


FIG. 5.—Number density evolution as a function of equivalent width. *Solid lines*, lines with $W_{\lambda_0} \geq 0.24$ Å; *dashed lines*, absorbers with $W_{\lambda_0} \geq 0.36$ Å; *dotted lines*, absorbers with $0.24 \leq W_{\lambda_0} < 0.36$ Å. Note marginally different slopes for weak and strong lines. Data are binned for presentation; the fits are to unbinned data.

that has combined width greater than the threshold (" blending-in "). These two effects work in opposite directions, and they are hard to quantify, especially in spectra with limited resolution (see, e.g., Parnell & Carswell 1988; Liu & Jones 1988). If the first of those two effects dominates over the second, the result may appear as if there were more strong lines at higher redshifts.

3.2.4. *Variation in $d\mathcal{N}/dz$ from Quasar to Quasar*

Impey et al. (1999) reported marginal evidence for quasar-to-quasar variations in the number density of lines in their sample of 10 spectra taken with *HST*/GHRS. Our sample, which contains 165 lines of sight, is particularly well suited to test whether there is structure in the distribution of Lyα absorbers on very large scales. We find remarkably little scatter in the number of lines detected. For each object, we calculated the expected number of absorption lines by integrating equation (1) over the usable parts of the spectrum and compared it with the number of lines observed in the spectrum. Figure 6 shows the histogram of the deviations in units of the individual uncertainties. Since the number of lines in each object can be small, the individual uncertainties were calculated using the Gehrels (1986) approximation, $\sigma_{\mathcal{N}} = 1 + (\mathcal{N} + 3/4)^{1/2}$, where $\mathcal{N}$ is the predicted number of lines. If the distribution were random, then the histogram would be a Gaussian with unit sigma. A dotted line in Figure 6 shows the predicted Gaussian distribution. The observed distribution is in fact much *narrower* than random: the farthest outliers deviate by only 2 σ, and there are only a handful of objects outside ± 1 σ.

The explanation is that the deviations in the number of lines detected in the FOS spectra is not given by counting statistics. Rather, the deviations reflect the uniformity of the intergalactic medium averaged over large scales. The size scale probed is given roughly by the Δz between Lyα and Lyβ emission lines of each quasar, or $\sim 750\ h_{50}^{-1}$ Mpc at $z = 1$ and $\sim 850\ h_{50}^{-1}$ Mpc at $z = 0.5$ ($q_0 = 0.5$).

We will explore the uniformity of the line distribution in more detail in a future paper.

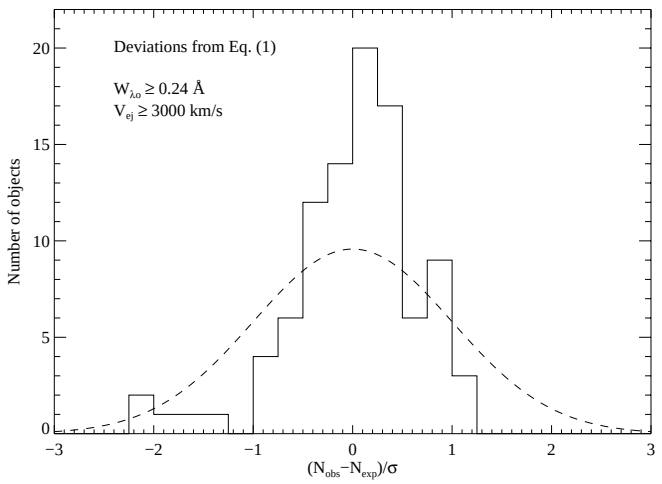


FIG. 6.—Histogram of deviations of observed number of lines in individual objects from the expected number of lines, expressed in units of individual uncertainties for each object. The expected number of lines was calculated by integrating eq. (1) over the available regions of spectra. Dashed line shows a Gaussian distribution with unit σ, normalized to the size of the sample.

3.2.5. *Line Equivalent Width and Neutral Hydrogen Column Density Distributions*

Equation (1) describes very well the distribution of rest equivalent widths of lines in the sample. We note, however, that the derived value of the equivalent width distribution parameter, $W_\star$, depends quite strongly on whether Lyα lines associated with metal systems are included in the analyzed sample. Figure 7 shows the distribution of equivalent widths in the $W_{\lambda_0} \geq 0.24$ Å, $V_{ej} \geq 3000$ km s^{-1} samples. Clearly, inclusion of lines from metal systems, which (as noted above) tend to be strong, affects the slope of the observed distribution.

It has been found that a simple power law, $d\mathcal{N}/dN_{\rm H\,I} \propto N_{\rm H\,I}^{-\beta}$, describes the distribution of Lyα forest column densities $N_{\rm H\,I}$. Analyses of high-redshift data (Petitjean et al. 1993; Press & Rybicki 1993; Hu et al. 1995; Dobrzycki & Bechtold 1996; Kim et al. 2001) showed that the value of β is in the 1.4–1.7 range. Analysis of low-redshift data from *HST*/GHRS (Penton et al. 2000) indicated β near the high end of this range, at 1.7–1.8. However, recent analysis by Davé & Tripp (2001) of high-resolution *HST*/STIS spectra of two quasars suggested that at low z the distribution is even steeper, with $\beta \approx 2.0$.

The FOS data lack the spectral resolution to perform direct Voigt profile fitting, which is necessary to derive the column density directly. However, because of the large size of the sample we can obtain precise measurements of the equivalent width distribution. Since column density and equivalent width are related via the curve of growth (see, e.g., Barcons & Webb 1991; Chernomordik & Ozernoy 1993; Penton et al. 2000), the distribution of line equivalent widths can give insight into the distribution of column densities.

Our data do not support the $\beta \approx 2$ value of the column density distribution slope. For all our Lyα forest subsamples, we get the equivalent width distribution parameter, $W_\star$, in the 0.20–0.22 Å range with very low uncertainties, of the order of 0.01 Å or less. This value of $W_\star$, when converted to the value of β using the curve of growth, yields $\beta \leq 1.6$–1.7, depending on the Doppler parameter distribution. In order to obtain the value of the slope in the vicinity

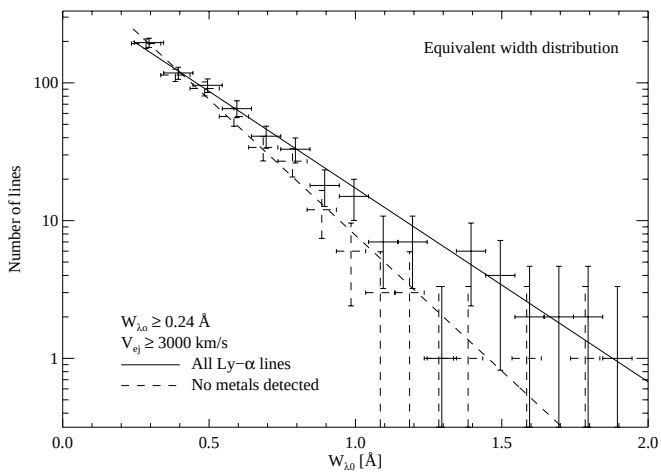


FIG. 7.—Distribution of rest equivalent widths in the $W_{\lambda_0} \geq 0.24$ Å, $V_{ej} \geq 3000$ km s^{-1} sample. The solid line shows the data points and the fit of $d\mathcal{N}/dW_{\lambda_0} \propto \exp(-W_{\lambda_0}/W_\star)$ for all Lyα lines in the sample, the dashed line shows the data and fit for the Lyα forest lines only.

of 2, we would have to have $W_\star$ from the 0.10–0.13 Å range, which is inconsistent with our results.

However, as Barcons & Webb (1991) pointed out, the relation between β and $W_\star$ may be affected by a subtle problem with line blending, or the presence of clustering of weak lines. Since those effects are hard to quantify, it is possible that the discrepancy is in fact smaller. Also, as noted above, the derivation of $W_\star$ is rather sensitive to the selection criteria in the sample. Including/excluding lines associated with metal systems in the sample leads to a distinctly different value of the distribution slope. This may help explain some of the discrepancy with the Davé & Tripp (2001) result.

4. CLUSTERING IN THE *HST*/FOS SAMPLE

An important clue to the nature of the Lyα absorption in quasar spectra is the clustering of lines in redshift space. In general, it is agreed that a weak clustering at scales of few hundred km s^{-1} is present in high-redshift Lyα forest (Rauch 1998 and references therein; more recently Liske et al. 2000; Penton et al. 2000). At low redshifts, Ulmer (1996) analyzed the line clustering in the spectra of 12 objects from the *HST*/FOS Key Project (100 lines) and reported a significant excess of line pairs at velocity separations of 250–500 km s^{-1}. More recently, Vanden Berk et al. (1999) reported positive correlation for similar velocity separations, though not as strong as Ulmer, in a sample consisting of the combination of Ulmer's sample and FOS spectra of quasars in the galactic poles (217 absorption lines, 22 quasars); they noted that the signal seems to be coming from a small set of line "clumps" in a few of the objects.

Impey et al. (1999) found excess of nearest-neighbor pairs at separations of 250–500 km s^{-1} in their sample of 139 lines from 10 *HST*/GHRS spectra, but they did not find any correlation function signal on any scales. However, Penton et al. (2000) reported a clustering signal for $\Delta V \leq 150$ km s^{-1} in their sample of 15 *HST*/GHRS spectra containing 111 lines.

The critical factor in the analysis of line clustering is the number of the available objects (i.e., lines of sight), since correlating the line positions is possible only in one dimension. Our sample is a superset of the Ulmer sample and—with the exception of two quasars, TON 155 and 1306+3021, which did not meet our sample's criteria—of the Vanden Berk et al. sample. In our data set that has comparable selection criteria ($W_{\lambda_0} \geq 0.24$ Å, $V_{\rm ej} \geq 3000$ km s^{-1}), we have 84 objects with 622 absorption lines, i.e., 7 times more lines of sight and 6 times more lines than Ulmer and around 4 times more lines of sight and 3 times more lines than Vanden Berk et al.

4.1. Lyα–Lyα *Clustering*

We calculated the correlation function by comparing the observed number of pairs of lines with the number counted in Monte Carlo simulations. We performed the simulations by drawing redshifts at random from the power-law distribution of $d\mathcal{N}/dz$ (eq. [1]) inside ranges identical to those in which our sample was defined. Each simulation was run until we had a total number of lines equal to the total number of lines in the real sample. We ran the simulations 10,000 times. To account for blending, we removed pairs with separations smaller than 250 km s^{-1}. However, we do expect blending to play at least some role, so that the number of expected pairs in the simulations may be overestimated, primarily in the 250–500 km s^{-1} bin.

The clustering results in our sample are shown in Figure 8. Solid crosses show the observed number of pairs in each velocity separation bin, while the dashed histogram shows the expected number of pairs, as calculated through the simulations.

A key issue is the uncertainties of the observed data points. If the lines are clustered, simply taking the square root of the number of line pairs in each bin will cause the error of the bin to be underestimated. We calculated the error bars for the observed data points using a modified bootstrap technique, similar to the method used by Fernández-Soto (1996). In this method, one replaces parts of the spectra with randomly selected substitute parts of the spectra and then calculates the distribution of pairs, repeating this procedure a large number of times. It can be shown that the dispersion of pair counts in each bin is an unbiased estimate of the actual variance in this bin.

In Figure 8, a weak correlation can be seen for $\Delta V < 500$ km s^{-1}. The signal is weak, though—as mentioned above—it is quite possible that line blending was not all accounted for in the simulations, leading to overestimating the expected number of pairs, thus mitigating the clustering signal.

The correlation found in our data has lower amplitude than the one reported by Ulmer (1996) or Vanden Berk et al. (1999). At least part of the difference can be explained if one looks into the sample used by Ulmer (and, consequently, Vanden Berk et al.) in more detail.

We first note that our selection criteria excluded regions containing the cluster of four pairs in TON 153, since this region is blueward of the Lyβ emission line. In regions that we have in common, we note the following differences:

1. In PG 1352+011, Ulmer has four close pairs, coming from lines near 1843, 1846, 1849, 1852, and 1855 Å. We present this region in Figure 9. The line at 1843 Å was deblended by Key Project from a wing of a strong Si III line near 1841 Å. In our analysis (Paper III) it was not identified as a separate feature. We do see a line near 1849 Å (Paper III), but it has a detection significance of 2.7 σ, which is too

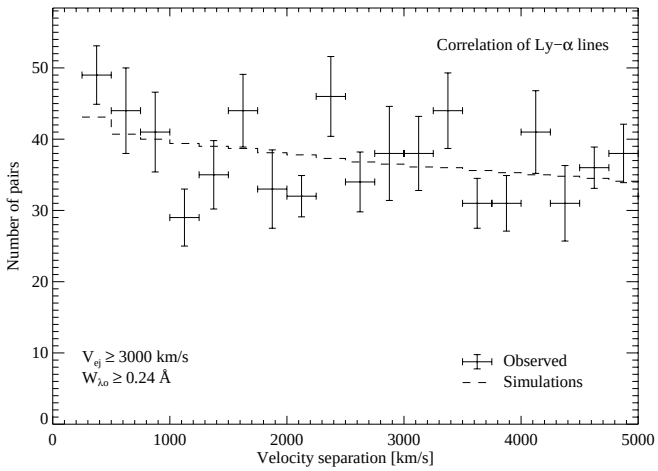


FIG. 8.—Observed (*solid crosses*) and expected (*dashed histogram*) number of pairs vs. velocity separation in the $W_{\lambda_0} \geq 0.24$ Å, $V_{\rm ej} \geq 3000$ km s^{-1} sample, including the metal systems. This plot is directly comparable to the lower panel of Fig. 1 of Ulmer (1996). Error bars were estimated using bootstrap technique, see text.

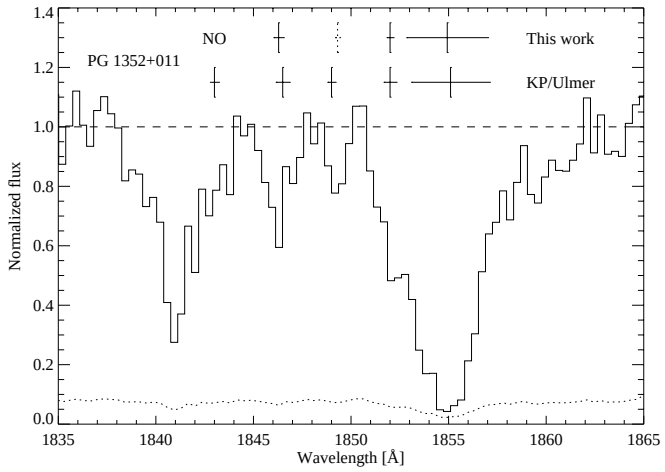


FIG. 9.—Region of the spectrum of PG 1352+011 where a difference between our analysis (Paper III) and the Key Project leads to a difference in the clustering signal. Dotted line shows 1 σ error in the spectrum. Upper row of crosses above absorption features represent our identifications, the lower crosses represent those of the Key Project. The dotted symbol denotes a line identified in Paper III, but at a significance too low to be included in our analysis. "NO" marks a location of a Key Project line that is not identified as a separate feature in our analysis. See text for discussion.

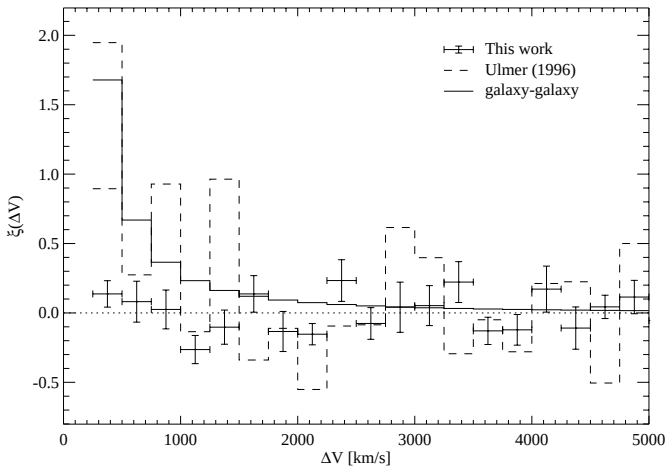


FIG. 10.—Two-point correlation function, $\xi(\Delta V)$, for our data (*solid crosses*), Ulmer (1996) (*dashed line*), and galaxy-galaxy correlation (*solid line*). Note two data points for Ulmer's data in the 250–500 km s^{-1} bin; the lower point indicates the correlation function one gets if one removes five disputable pairs from Ulmer's sample.

low to be included in the sample analyzed here. All these factors result in our sample only containing one close pair in this region, the 1852–1855 pair.

2. In two pairs in Ulmer's sample—$\lambda = 1562.7$ in 3C 351 and $\lambda = 2601.6$ in PG 1634+706—we identify one of the pair components as a heavy element line rather than as a Lyα line. This means that they are removed from consideration in our analysis of correlations. Both these systems were considered by Ulmer (and Vanden Berk et al.) to be Lyα pairs.

In total, in the regions that we had in common, we do see five fewer close pairs. Removal of those pairs lowers the number reported by Ulmer (14 pairs) by 36%, and the correlation signal (i.e., the ratio of $N_{\rm obs}/N_{\rm ran}$) by about half. Indeed, as it has been found in previous studies (Heisler, Hogan, & White 1989; Bahcall et al. 1996; Vanden Berk et al. 1999), the correlation signal is dependent on a small handful of line pairs.

In Figure 10 we show the results converted to the two-point correlation function, $\xi(\Delta V) = N_{\rm obs}/N_{\rm ran} - 1$. On the same plot, the dashed line shows Ulmer's result. We show two data points for Ulmer's results in the 250–500 km s^{-1} bin; the bottom one is what his result would be if the five close pairs mentioned above were removed. Please note that we examined in detail only the 250–500 km s^{-1} bin in Ulmer's data, and so we do not show how other velocity bins would be affected. Obviously, the differences in line identifications and deblending accounts for some—but not all—of the difference between the correlation strengths.

Clustering of Lyα lines at small velocity separations is predicted by cold dark matter (CDM) model simulations of the galaxy formation, the growth of large-scale structure, and subsequent evolution of the intergalactic medium (Cen et al. 1998; Davé et al. 1999). These models predict that the Lyα absorbing gas traces the dark matter distribution more closely than galaxies, and so the two-point correlation function of Lyα clouds provides a different and complementary constraint on the formation of large-scale structure than the distribution of galaxies and galaxy clusters. The solid histogram on Figure 10 shows the galaxy-galaxy correlation function, taken as $\xi_{\rm g-g} = (\Delta V/500)^{-1.8}$ (e.g., Davis & Peebles 1983). We see that the galaxy-galaxy correlation function is stronger than the Lyα correlation function, as is predicted by the CDM simulations.

4.2. Lyα–*Metal System Correlation*

Analyses of FOS data suggested that Lyα forest lines may have a tendency to be found preferably near heavy element systems. This tendency appeared to be even stronger if one considered the "extensive" metal systems, i.e., metal systems with four or more identified species; those systems were often seen near "clumps" of Lyα lines. See Bahcall et al. (1996), Jannuzi (1997), and Vanden Berk et al. (1999). Given scarcity of available systems, those analyses were, for the most part, qualitative, though Vanden Berk et al. reported some positive signal for metal system–Lyα forest correlation at $\Delta V = 1000$–1500 km s^{-1} for strong ($W_{\lambda_0} > 0.5$ Å) lines.

In the $W_{\lambda_0} > 0.24$ Å, $V_{\rm ej} \geq 3000$ km s^{-1} sample, we have 78 identified metal systems, 41 of which qualify as "extensive." We analyzed the correlation of Lyα forest versus those systems, using approach similar to the one used in the analysis of Lyα forest correlations. In the simulations, we fixed the positions of the metal systems at their observed locations and selected locations of Lyα forest lines at random. We compared the simulated and observed pairs of absorbers, requiring that one of the pair components be a metal system. We do not see any correlation on any scale in both cases (Fig. 11). It is, however, clear that even the entire FOS sample is somewhat too small for this test.

5. SUMMARY

We analyzed the redshift distribution of the Lyα clouds at $z = 0.0$–1.7 in the spectra of 165 quasars. The major results are the following:

1. We confirm that the clouds at redshifts less than 1.7 undergo slow, if any, evolution. A single power law is an excellent approximation of the behavior of the number den-

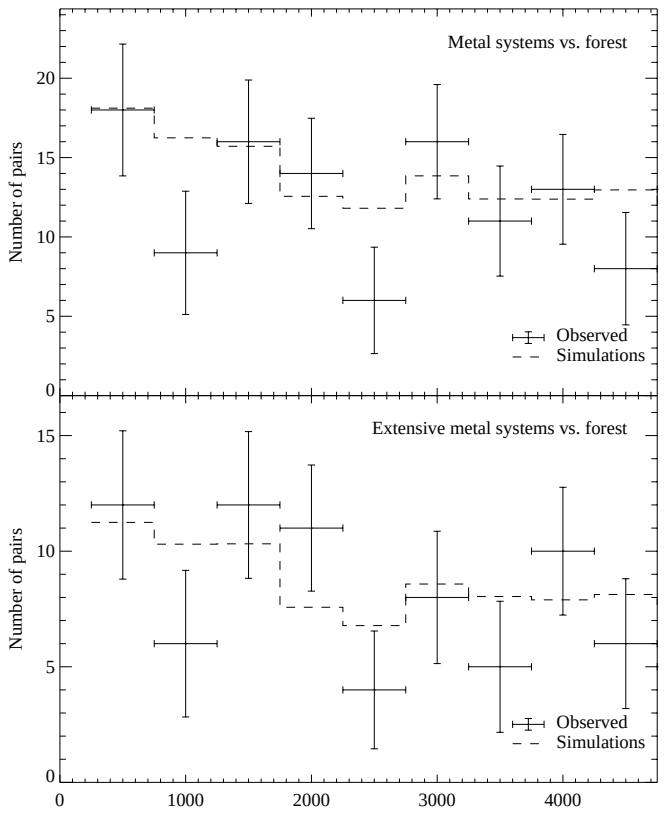


FIG. 11.—Distribution of line velocity separations, as in Fig. 8, between metal systems and Lyα forest lines. *Top panel*: Lyα forest lines vs. metal line systems. *Bottom panel*: Lyα forest vs. extensive metal systems.

sity evolution of lines at low redshift. However, we find the evolution of the cloud number density to be somewhat steeper that the one found by the *HST* Key Project, probably the result of a different proportion of $z \sim 1.5$–1.7 lines in the two samples.

2. We see marginal evidence for a difference between the evolution index for weak and strong lines. The weak lines undergo evolution in the opposite direction from the strong lines, i.e., their number per comoving volume increases with decreasing redshift. The strong lines are consistent with the no-evolution case.

3. The object-to-object variation in the number of lines is small, suggesting that the intergalactic medium is uniform on $\sim$800 Mpc scales.

4. We see weak clustering in the Lyα forest for $\Delta V \leq 500$ km s^{-1}. However, the correlation is weaker than reported by Ulmer (1996) or Vanden Berk et al. (1999). At least part of the difference can be accounted for by differences in details of the deblending and identification of a small number of absorption features. In all cases, the clustering signal is smaller than that seen for galaxies at the same redshift.

5. No correlations were found for Lyα forest versus metal systems and Lyα forest versus "extensive" metal systems, although the numbers are small, and the limits correspondingly are weak.

The FOS data set is useful for many other quasar absorption line studies. Paper V reports the analysis of the proximity effect, and the evolution of the UV radiation field which may drive the evolution of $d\mathcal{N}/dz$ for the Lyα forest clouds derived here (see Paper V and references therein for further discussion of this point). The results for clustering described in this paper can be confirmed or refuted with high-resolution spectroscopy, currently planned or underway with STIS on board *HST*.

A. D. would like to thank A. Fernández-Soto for helpful comments on the bootstrapping technique. We would like to thank the anonymous referee for several helpful comments. This research has made use of the NASA/IPAC Extragalactic Database (NED), which is operated by the Jet Propulsion Laboratory, California Institute of Technology, under contract with NASA. This project was supported by STScI grants AR-05785.02-94A and GO-06606.01-95. A. D. acknowledges support from NASA Contract NAS8-39073 (CXC). J. B., J. S., and M. M. received financial support from NSF grant AST-9617060. J. S. acknowledges support of the National Science Foundation Graduate Research Fellowship and the Zonta Foundation Amelia Earhart Fellowship.

REFERENCES

Bahcall, J. N., et al. 1993, ApJS, 87, 1
———. 1996, ApJ, 457, 19
Bajtlik, S., Duncan, R. C., & Ostriker, J. P. 1988, ApJ, 345, 39
Barcons, X., & Webb, J. K. 1991, MNRAS, 253, 207
Bechtold, J. 1994, ApJS, 91, 1
Bechtold, J., Dobrzycki, A., Wilden, B., Morita, M., Scott, J., Dobrzycka, D., Tran, K.-V., & Aldcroft, T. A. 2002, ApJS, 140, 143, in press (Paper III)
Cen, R., Phelps, S., Miralda-Escudé, J., & Ostriker, J. P. 1998, ApJ, 496, 577
Chernomordik, V. V., & Ozernoy, L. M. 1993, ApJ, 404, L5
Davé, R., Hernquist, L., Katz, N., & Weinberg, D. H. 1999, ApJ, 511, 521
Davé, R., & Tripp, T. M. 2001, ApJ, 553, 528
Davis, M., & Peebles, P. J. E. 1983, ApJ, 267, 465
Dobrzycki, A., & Bechtold, J. 1996, ApJ, 457, 102
Fernández-Soto, A. 1996, Ph.D. thesis, Univ. de Cantabria
Ford, H. C., & Hartig, G. F. 1990, Faint Object Spectrograph Instrument Handbook (Baltimore: STScI)
Gehrels, N. 1986, ApJ, 303, 336
Heisler, J., Hogan, C. J., & White, S. D. M. 1989, ApJ, 347, 52
Hu, E. M., Kim, T., Cowie, L. L., Songaila, A., & Rauch, M. 1995, AJ, 110, 1526
Impey, C. D., Petry, C. E., & Flint, K. P. 1999, ApJ, 524, 536
Jannuzi, B. T. 1997, in Proc. 13th IAP Colloquium, Structure and Evolution of the IGM from QSO Absorption Line Systems, ed. P. Petitjean & S. Charlot (Paris: Editions Frontiéres), 93
Jannuzi, B. T., et al. 1996, ApJ, 470, L11
Jannuzi, B. T., et al. 1998, ApJS, 118, 1
Kim, T.-S., Cristiani, S., & D'Odorico, S. 2001, A&A, 373, 757
Kim, T.-S., Hu, E. M., Cowie, L. L., & Songaila, A. 1997, AJ, 114, 1
Liske, J., Webb, J. K., Williger, G. M., Fernández-Soto, A., & Carswell, R. F. 2000, MNRAS, 311, 657
Liu, X. D., & Jones, B. J. T. 1988, MNRAS, 230, 481
Lu, L., Wolfe, A. M., & Turnshek, D. A. 1991, ApJ, 367, 19
Murdoch, H. S., Hunstead, R. W., Pettini, M., & Blades, J. C. 1986, ApJ, 309, 19
Parnell, H. C., & Carswell, R. F. 1988, MNRAS, 230, 491
Penton, S. V., Shull, J. M., & Stocke, J. T. 2000, ApJ, 544, 150
Peterson, B. A. 1978, in IAU Symp. 79, The Large Scale Structure of the Universe, ed. M. S. Longair & J. Einasto (Dordrecht: Reidel), 389
Petitjean, P., Webb, J. K., Rauch, M., Carswell, R. F., & Lanzetta, K. 1993, MNRAS, 262, 499
Press, W. H., & Rybicki, G. B. 1993, ApJ, 418, 585
Rauch, M. 1998, ARA&A, 36, 267
Schneider, D. P., et al. 1993, ApJS, 87, 45
Scott, J., Bechtold, J., & Dobrzycki, A. 2000, ApJS, 130, 37 (Paper I)
Scott, J., Bechtold, J., Dobrzycki, A., & Kulkarni, V. 2000, ApJS, 130, 67 (Paper II)
Scott, J., Bechtold, J., Morita, M., Dobrzycki, A., & Kulkarni, V. 2002, ApJ, 571, 665, in press (Paper V)
Ulmer, A. 1996, ApJ, 473, 110
Vanden Berk, D. E., et al. 1999, ApJS, 122, 355
Weymann, R. J., et al. 1998, ApJ, 506, 1